Dilatometric study of high silicon bainitic steels: Solid-state transformations

G.M.A.M. El-Fallah

School of Engineering, University of Leicester, Leicester, LE1 7RH, UK

ARTICLE INFO

ABSTRACT

High silicon bainitic steels have gained significant recognition in various applications due to their exceptional properties, such as high strength, favourable corrosion resistance, and excellent high-temperature stability. This study investigates an alloy capable of generating a finer bainitic structure through a transformation at 260 °C, leading to the desired microstructure. Interestingly, other phenomena were discovered while pursuing optimal heat treatment conditions. At temperatures exceeding 850 °C, the alloy exhibits a tendency for graphite formation, which has intriguing implications for its mechanical properties. The high silicon concentration in the alloy significantly retards cementite growth, resulting in a microstructure composed solely of bainitic ferrite and residual austenite through the transformation of austenite below the bainite start temperature. Furthermore, it is observed that pearlite formed during rapid transformation at 650 °C does not exhibit the predicted equilibrium chemical composition. This discrepancy challenges the existing models of pearlite growth, which assume local equilibrium at the shared interface with austenite. This research aims to investigate the influence of silicon content on solid-state transformations in high-silicon steels using dilatometry, optical microscopy, scanning electron microscopy, and X–ray diffraction techniques. These analytical methods will provide insights into the intricate processes occurring during isothermal transformation temperatures, contributing to a deeper understanding of the material's behaviour and its potential applications.

1. Introduction

A wide variety of the physical properties of steels can be obtained by carefully controlling the processing conditions. This is one of the main reasons, along with low production costs, that makes steel the most widely used amongst the metals. Nevertheless, the production of steel is extremely polluting in terms of CO_2. Developments that improve the mechanical properties of steel without increasing the cost of production would not only allow a reduction in the consumption of steel but also would result in a positive impact on the environment. During processing it is common for steel to be heated to temperatures in excess of 1000 °C, so that austenite, which has a face-centred cubic crystal structure is generated. Various phase changes occur when the steel is then cooled to ambient temperatures. In particular, at temperatures below about $\sim$ 900 °C, a body-centred cubic structure called ferrite becomes stable. These changes in stability as a function of temperature, and indeed of chemical composition and processing, can be exploited to control the structure and properties of steels. Moreover the changes can occur by a variety of atomic mechanisms so that the palette of microstructures available becomes quite extensive, more so than many other common metallic systems.

Transformations where diffusion is not an essential are accomplished by the concerted motion of atoms, leading to systematic displacements [1]. The transformation of austenite into bainite falls in this regime of limited atomic mobility, enabling the growth of bainite plates without diffusion, although carbon may undergo redistribution or precipitation post-transformation. A notable outcome of this displacive mechanism is the formation of thin bainite plates, which naturally refines the grain structure without necessitating any thermomechanical processing. This makes the bainitic steels strong and tough, as long as cementite precipitation is prevented. The addition of silicon plays a crucial role in this regard by impeding cementite precipitation [2–4], such that carbon partitioning from the supersaturated bainitic ferrite occurs in the residual austenite, which is then retained to enhance toughness. Alloy design is facilitated by solutes like nickel, which impact the hardenability and toughness of steel [5,6]. Furthermore, bainite ferrite plates become even thinner as the transformation temperature decreases [7,8], serving as the foundation for the development of nanostructured bainitic steels, as described in this paper [9,10].

Bulk nanocrystalline bainitic steels have recently been developed in which the austenite is much more resistant to thermal decomposition [11–13]. This work presents a detailed structural characterisation of this

Table 1
Chemical composition of the steel investigated, wt%.

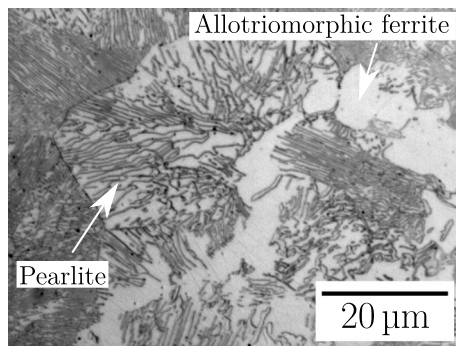| C	Si	Ni	Al	Mo	Mn	Co	Cr	Fe
0.72	3.87	3.40	1.39	0.21	0.02	<0.01	<0.01	balance

Fig. 1. Optical micrographs in as - received condition, the bright areas are allotriomorphic ferrite, which formed first, followed by pearlite.

alloy, with a specific emphasis on the formation of bainitic structures at varying isothermal transformation temperatures, using dilatometric analysis, optical microscopy, scanning electron microscopy, and X-ray diffraction. The overarching aim of this investigation is to gain a comprehensive understanding of the distinct structures that emerge during the transformation process and evaluate the feasibility of achieving a bainitic structure in high silicon bainitic steels.
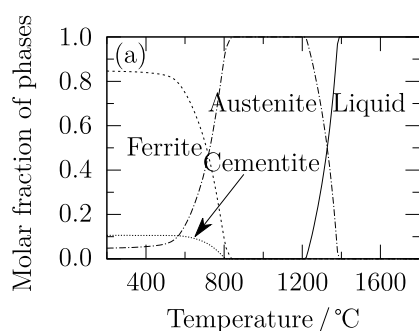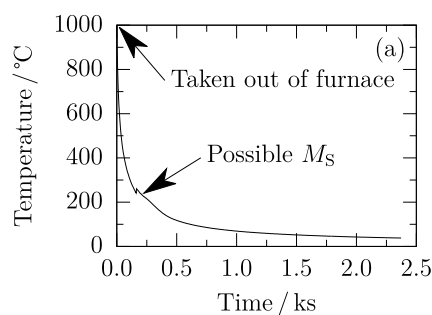
2. Materials and methods

The chemical composition of the alloy studied is listed in Table 1. The alloy was designed to generate a mixed nanostructure of bainitic ferrite plates embedded in a matrix of carbon-enriched austenite. The alloy has enough carbon and nickel to ensure the low transformation temperatures to achieve the nanostructure. However, the amount of silicon in this alloy is significantly higher than the usual amounts found in alloys of this kind, which suppresses the formation of cementite precipitation. Furthermore, the reduced concentration of manganese prevents the need for long transformation times, thereby facilitating the formation of the mixed nanostructure through elementary hardenability considerations. The alloy also has a high concentration of aluminium, which significantly accelerates the bainite transformation [14]. In addition, small amounts of molybdenum have been added to prevent any possibility of phosphorus-induced embrittlement of the austenite grain boundaries [15].
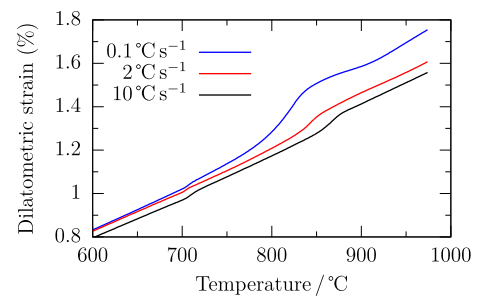

Fig. 4. Dilatometry curves during heating of initially pearlitic microstructure. The expansions observed at lower temperatures are due to austenite formation, while those occurring at higher temperatures are due to graphite formation. The extent of the later expansion becomes notably prominent at a slower heating rate.
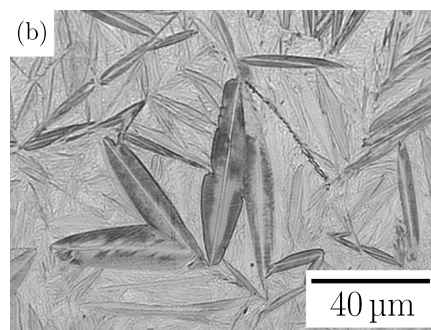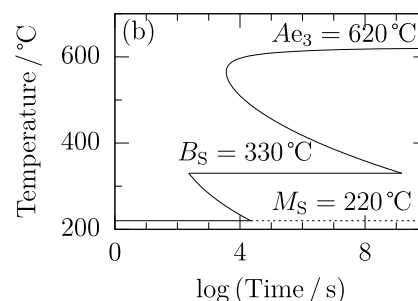

Fig. 2. (a) Equilibrium phase fractions were calculated over a range of temperatures using MTData [19,20] for the composition of as - received conditions. Liquid, austenite, ferrite and cementite phases are allowed to exist in the calculations. (b) TTT curve calculated using MTTTData [19,21,22]. The calculations predict that bainite will form in the temperature range of 220 °C–330 °C during isothermal transformation.

Fig. 3. (a) Temperature - time profiles for samples cooled in air after austenitisation, showing a change in gradient at ≈ 240 °C. (b) Martensitic microstructure formed cooled in air from 1000 °C to ambient temperature.
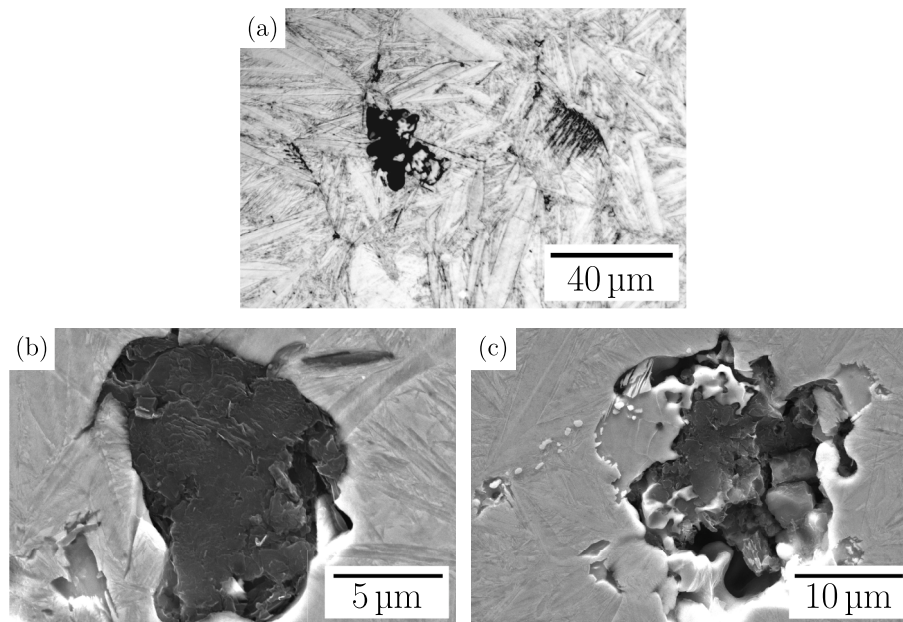
Fig. 5. Microstructures of the alloy after heating up to 1000 °C at 0.1 °C s^{-1}, showing (a) mostly martensite with nodular graphite and a small quantity of Widmanstätten ferrite at prior austenite grain boundaries. (b) Graphite nodule in a martensitic matrix. (b) Void caused by graphite dissolution.
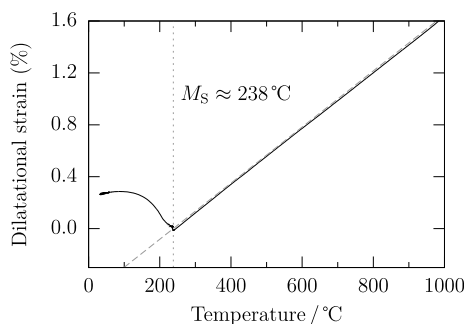

Fig. 6. Dilatometric curve of the alloy cooled at 5 °C s^{-1}, showing the M_S temperaturer according to the offset method with 1 vol.% transformation [24].

The alloy was produced as a 54 kg steel cast and forged to a final cross-section 57 mm × 83 mm with a 7:1 reduction ratio. Dilatometric samples 3 mm and length 10 mm were performed in a Bähr DIL 805 A dilatometer. Temperature, diameter and change in length were monitored.

Vickers hardness was measured with a 10 kg load on an ATM Qness 30+ automatic indenter, taking the average of ten indents in each case. The standard deviation (*STDEV*) of the measurement was taken to calculate the statistical standard error ($STDEV/\sqrt{N}$), where, N is the total number of indentations made.

Samples mounted in conductive bakelite were ground using silicon carbide emery papers (1200-grade to 2500-grade), followed by polishing with to 6 μm, 1 μm finishes using diamond paste, finishing with 0.25 μm colloidal silica for scanning electron microscopy on a FEI Nova NanoSEM operating at 15 kV. Etching was with a 2% nitric acid, 98% methanol mixture.

Samples for the X-ray analysis were ground and electropolished using 5% perchloric acid, 25% glycerol and 70% ethanol at 11 V for 8 min. X-ray diffraction analysis (Bruker D8 DAVINCI, Cu Kα radiation) was used to determine the fraction of retained austenite (V_γ). The machine was operated with a step size 0.050° with dwell time of 5 s, 2.5° primary slit, a divergence slit 8 mm wide and 18 mm antiscatter slit at 40 kV and 40 mA and a rotational speed was 30° min^{-1}. The results were subjected to

Rietveld refinement [16]. The weighted profile R-factor (R_{wp}) and goodness-of-fit were used to assess the quality of fitting, which also checked graphically [17]. The Dyson and Holmes [18] relationship between the austenite composition and its lattice parameter was used to estimate its carbon content (C_γ).

3. Results and discussion

Experiments were initiated to assess the transformation characteristics of the alloy. Introductory investigations were directed to evaluate the cooling and heating method required to form nanostructured bainitic steels and comprehensive dilatometric experiments were performed to study the transformation kinetics.

3.1. Initial experiments

The as-received state of the alloy has a microstructure that is a mixture of allotriomorphic ferrite and pearlite (Fig. 1), with a Vickers hardness of 461 ± 3 HV10, taking the average of ten indents.

Phase fractions were calculated using MTData [19,20], the alloy is predicted to be completely austenitic between 850 °C and 1220 °C, Fig. 2a. Thermodynamic modelling using MTTTData [19,21,22] indicated that the reconstructive transformations can be avoided if the alloy cooled to ≈ 600 °C in roughly 30 min (Fig. 2b). This shows the high hardenability which is necessary in the production of large components.

3.2. M_S temperature

The test, in which the alloy was austenitised and air cooled to ambient temperature revealed a change in gradient of the temperature profile at around 240 °C (Fig. 3a), corresponding to the martensitic transformation (Fig. 3b), consistent with $M_S = 220$ °C using MTTTData.

3.3. Experimental study on the effects of heating rates

The dilatometric curves of the as-received pearlitic material were examined at different heating rates to determine the optimal heating rate, as shown in Fig. 4. These curves exhibited two different expansions during the heating to 1000 °C, at ≈ 730 °C and ≈ 850 °C. The first
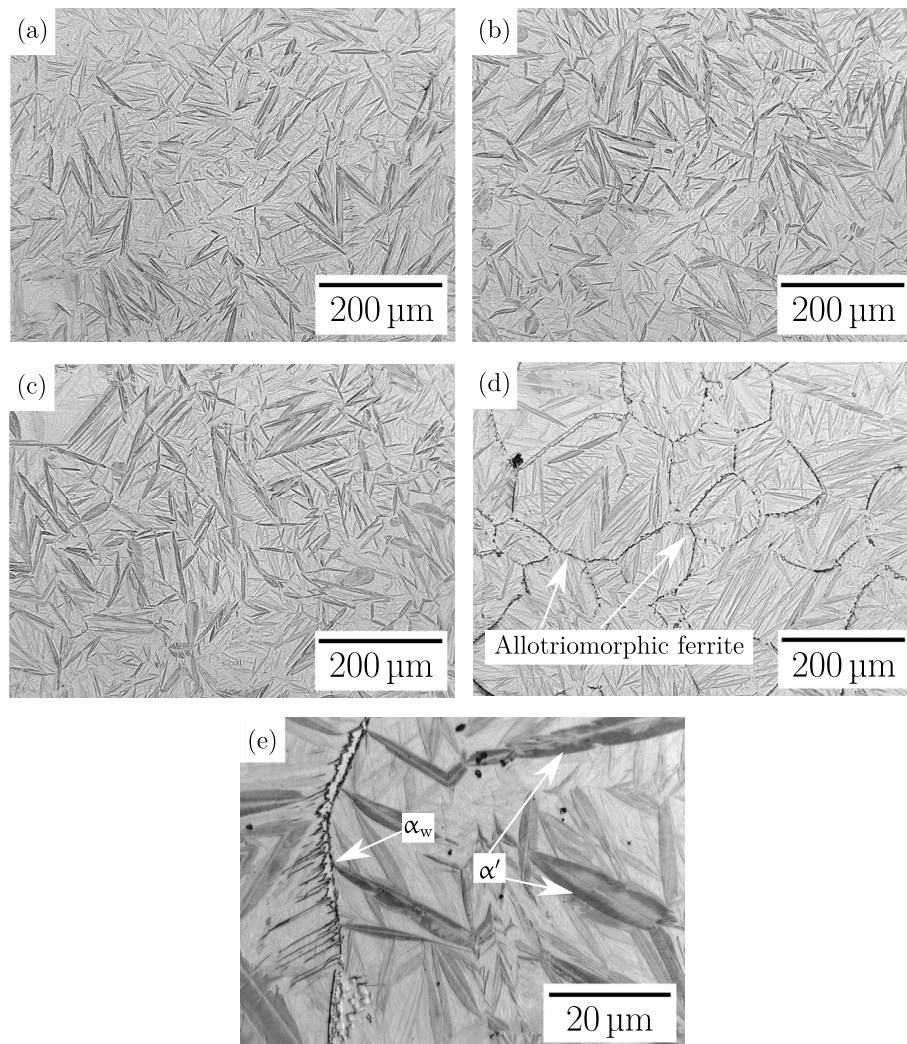
Fig. 7. Optical micrographs of martensitic structure, α', formed in the alloy cooled to ambient temperature at (a) 20 °C s^{-1}, (b) 10 °C s^{-1}, (c) 5 °C s^{-1} and (d) and (e) 2 °C s^{-1}. Cooling at 2 °C s^{-1} results in a small quantity of allotriomorphic and Widmanstätten ferrite, α_w.
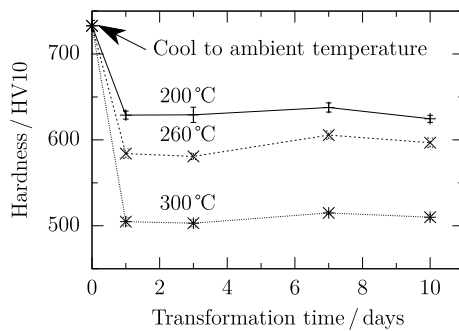
Fig. 8. Hardness of the alloy after austenitisation at 1000 °C for 30 min then transformed isothermally at 200 °C, 260 °C and 300 °C for different times as indicated.

expansion is due to austenite formation, indicating that the alloy is predominantly austenitic at 730 °C. The second expansion corresponds to the graphite formation.

It is worth noting that while the second expansion was observed across all heating rates, it became significantly more distinct at a slower heating rate (i.e., 0.1 °C s^{-1}). This can be attributed to the extended opportunity for the carbon atoms to diffuse and segregate, allowing for the growth of larger graphite flakes, Fig. 5. Conversely, no signs of graphite at higher heating rates (1–10 °C s^{-1}). This suggests that the thermal energy input rate profoundly impacts graphite's precipitation kinetics and subsequent distribution within the material. Furthermore, the temperature at which decomposition was first detected increased with higher heating rates, as shown in Fig. 4.

This phenomenon indicates a critical transition in the microstructural evolution, marking the initiation of graphite precipitation. The presence of graphite within the alloy has significant implications for its mechanical and thermal behaviour, as the inclusion of graphite can influence its strength, ductility, and thermal conductivity [23]. Considering that the presence of graphite reduces the amount of carbon available for subsequent transformations, a heating rate of 5 °C s^{-1} has been chosen for further investigations.

Table 2
Heat - treatment conditions applied in dilatometry experiments.

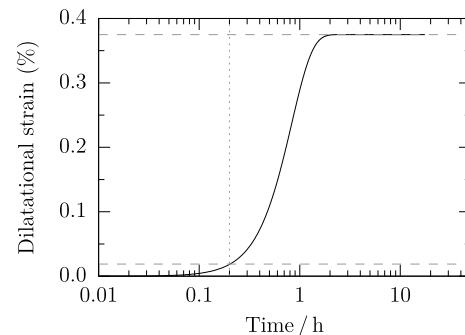| Temperature / °C	800	750	700	650	600	550	500
Hold time / h	5.0	5.0	5.0	5.0	6.0	6.5	6.5
Temperature / °C	450	400	350	325	300	275	260
Hold time / h	12.0	12.0	12.0	12.0	12.0	12.0	12.0
Temperature / °C	30	30	30	30			
Cooling rate / °C s^{-1}	20	10	5	2			

Fig. 10. Alloy transformed at 260 °C. Horizontal lines are fitted to the "start" and "end" of the transformation.

3.4. Experimental determination of martensite start temperature

Transformation temperatures were determined by slope changes in the dilatometric curve, using the offset method [24]. The alloy was austenitised at 1000 °C for 30 min and then quenched to ambient temperature to determine, $M_S = 238$ °C for cooling at 5 °C s^{-1} (Fig. 6) to ensure the austenite is untransformed before reaching M_S. Cooling at lower rates (i.e. ≤ 2 °C s^{-1}) permits some allotriomorphic and Widmanstätten ferrite to form (Fig. 7).
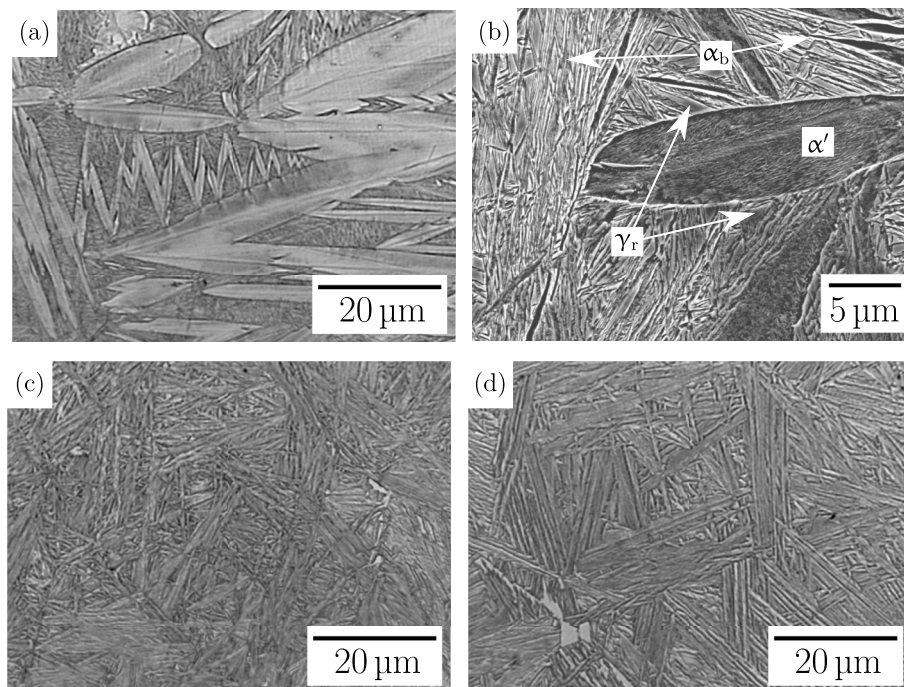

Fig. 9. Optical microstructures of the alloy after austenitisation at 1000 °C for 30 min and isothermally transformed for 24 h at (a) and (b) 200 °C, bainite structure between large martensite plates. (c) 260 °C and (d) 300 °C, both temperatures result in substantial quantities of bainite.
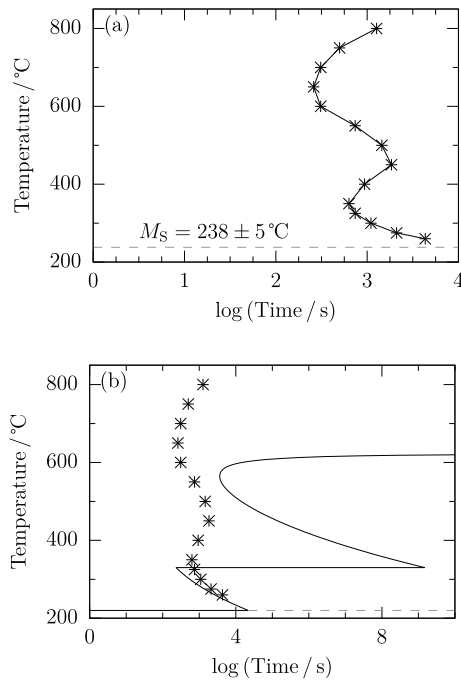
Fig. 11. (a) Measured TTT diagram based on the times required for the transformation at every temperature. (b) Comparison of experimental and measured transformation start times (points) and those calculated (lines) using MTTTData [19,21,22].

Table 3
Structures formed in the alloy and associated hardness data.

Temperature / °C	Transformation Start Time / s	Microstructure	Hardness HV10
800	1270	Ferrite, graphite, martensite	300 ± 18
750	500	Ferrite, graphite	290 ± 6
700	310	Ferrite, graphite	272 ± 7
650	260	Ferrite, cementite	451 ± 7
600	310	Ferrite, cementite	475 ± 7
550	740	Bainite, cementite, ϵ	488 ± 5
500	1450	Bainite, austenite, cementite, ϵ	434 ± 7
450	1849	Bainite, austenite, cementite, ϵ	487 ± 8
400	936	Bainite, retained austenite	430 ± 6
350	632	Bainite, retained austenite	489 ± 5
325	740	Bainite, retained austenite	511 ± 4
300	1100	Bainite, retained austenite	548 ± 6
275	2100	Bainite, retained austenite	562 ± 4
260	4328	Bainite, retained austenite	589 ± 3
2 °C s^{-1}	N/A	Martensite, allotriomorphic ferrite	717 ± 11
5 °C s^{-1}	N/A	Martensite	721 ± 8
10 °C s^{-1}	N/A	Martensite	737 ± 6
20 °C s^{-1}	N/A	Martensite	753 ± 9

recalescence detected during cooling (Fig. 3). The samples transformed at 260 °C and 300 °C, however, showed the expected combination of bainitic ferrite and retained austenite (Figs. 9c and d). These results will be explained later (Section 3.7).

3.5. Transformation kinetics

Samples were austenitised at 1000 °C for 30 min, freely cooled and transformed isothermally at 200 °C, 260 °C and 300 °C for different times, giving the hardness values shown in Fig. 8. The hardness becomes steady after 1 d at all temperatures, suggesting that the subsequent microstructural changes are small. Lower transformation temperatures achieve higher hardness, consistent with the expected finer bainitic microstructure [25].

The samples transformed at 200 °C consisted of a mixture of bainite and large martensite plates. The martensite plates are a lot bigger than the bainite and have formed in typical self-accommodating zig-zag chains (Fig. 9a). Lots of martensite plates expand to the prior austenite grain boundaries, indicating that they formed first to be followed by bainite (Fig. 9b). Therefore M_S must be above 200 °C consistent with the
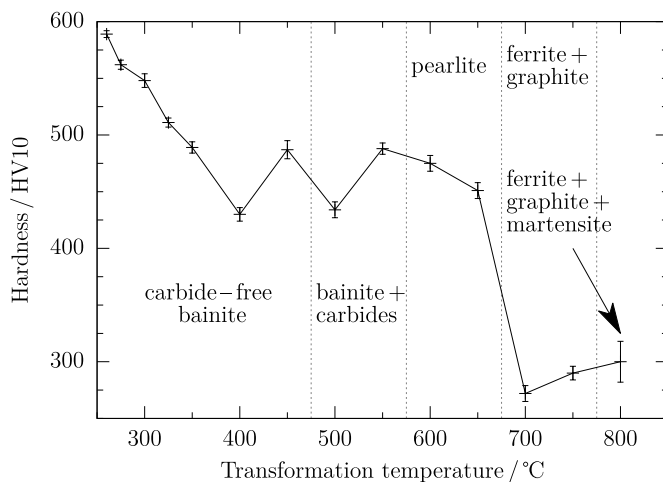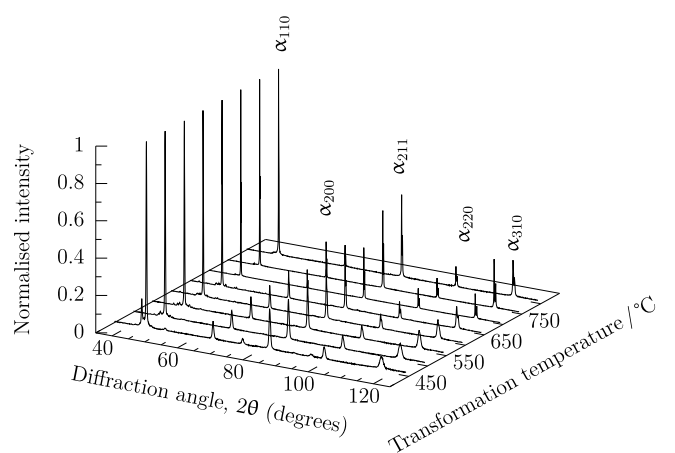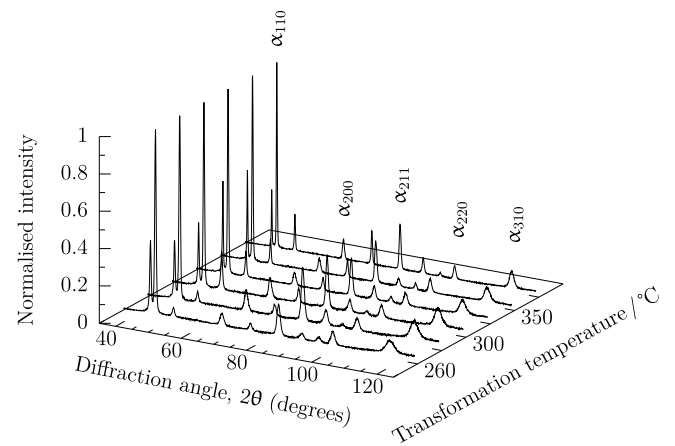

Fig. 12. Hardness and evaluated microstructure for isothermally transformed alloy.

Fig. 13. X - ray diffractograms after isothermal transformation. For the sake of clarity only ferrite peaks are labelled, other peaks may be seen in Fig. 24.
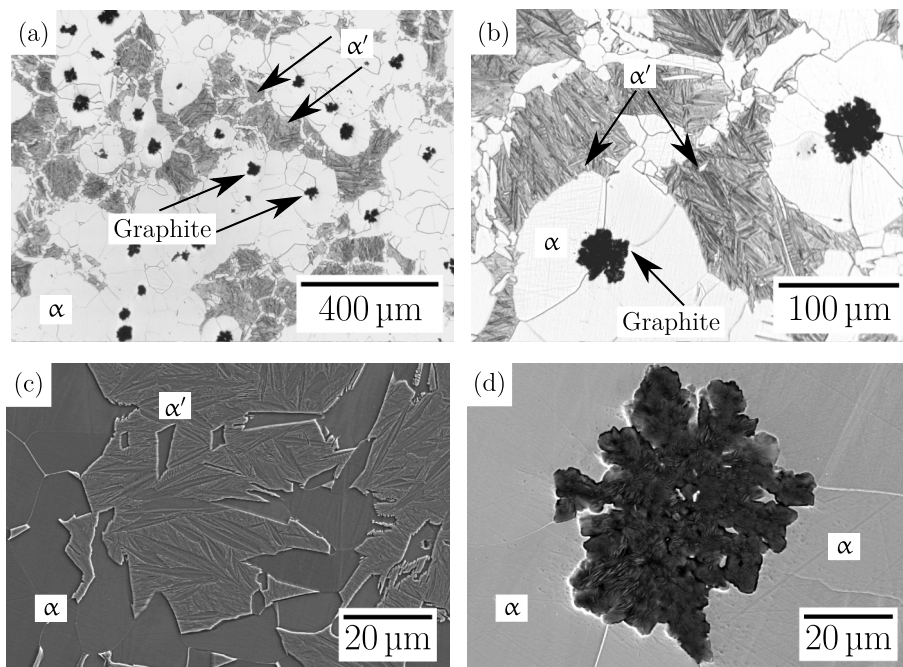
Fig. 14. Alloy isothermally transformed at 800 °C for 5 h. (a) and (b) optical micrographs. Scanning electron micrograph of (c) martensite plates in ferrite 'α' and (d) graphite nodules in a ferritic matrix.
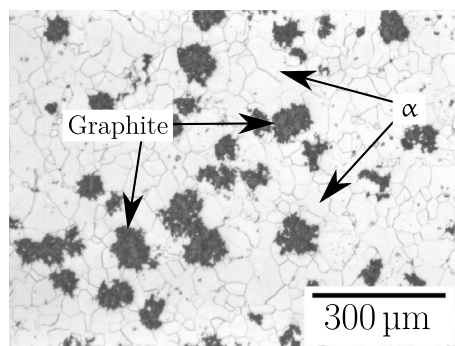

Fig. 15. (a) Graphite in a ferritic matrix in "blackheart cast iron" held at 900 °C for many days before cooling slowly to grow graphite nodules [[29], micrograph 795].

3.6. Dilatometric study of phase transformations

All dilatometry samples were similarly heated at 5 °C s^{-1} under vacuum to 1000 °C where they were held for 30 min. Samples then were either transformed isothermally or cooled continuously at 5 °C s^{-1} to ambient temperature, as detailed in Table 2. Samples were isothermally transformed at various temperatures, showing that reconstructive transformations were avoided. Zero time is defined when the isothermal temperature is reached, and the onset of. Transformation was then taken to begin when the strain had increased by 1% of the net change during the isothermal hold (Fig. 10).

Transformations measured in the alloy are rapid (Fig. 11a): an order of magnitude shorter time than earlier bulk nanostructured bainitic steels [e.g., Refs. [26–28]]. This is because of the absence of manganese, which decreases transformation driving force. Fig. 11b indicates that MTTTData predicts the correct bainite transformation times.

3.7. Transformation microstructures

The transformation products of the experimental isothermal transformations were assessed dilatometrically, optical and scanning electron

microscopy, hardness measurement Fig. 12, Table 3 and X – ray diffractometry Fig. 13. The isothermal transformation temperatures will be studied individually in the following sections.

3.7.1. 800 °C

The microstructure consisted of large ferrite grains containing irregular nodules of graphite together with some martensite, Fig. 14, due to the decomposition of the austenite which remains untransformed at 800 °C. Rietveld analysis (not including graphite) shows (79 ±3) vol.% ferrite and (21 ±5) vol.% austenite, consistent with equilibrium calculations of 75 vol.% ferrite, 22 vol.% austenite and 3 vol.% graphite. It was not possible to identify graphite using X-ray diffraction, however the microstructural appearance (Fig. 14a [1]) is typical of graphite seen in "blackheart cast-iron" (Fig. 15a). The graphite is a consequence of the well-known effect of a large silicon concentration in making cementite

---

[1] The structure looks like that of blackheart cast-ion which requires many days to remove the cementite and converted into graphite however, this take a very short time to produce a similar structure, albeit for much lower carbon concentration.
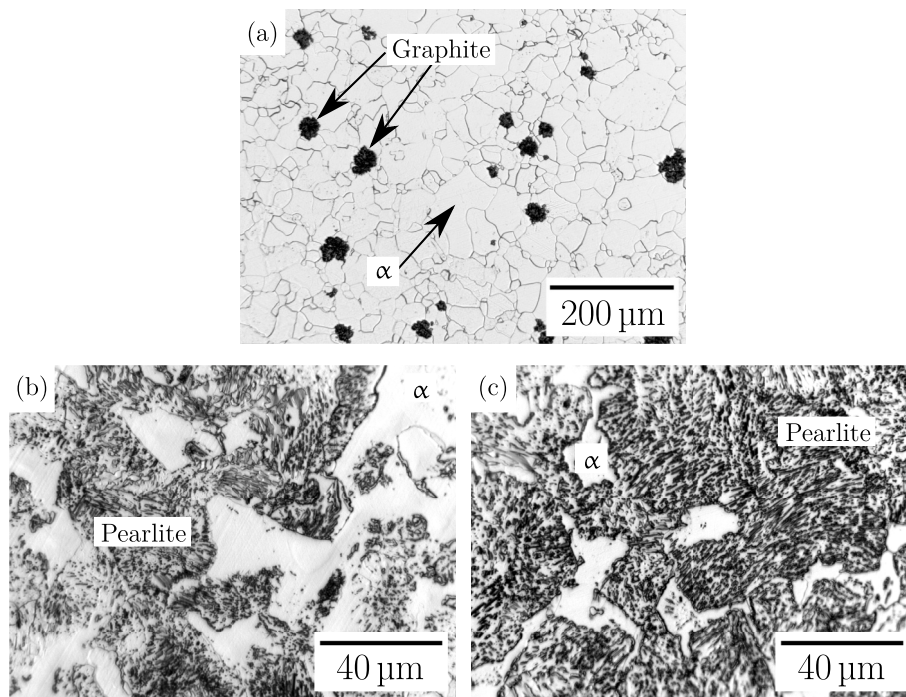
Fig. 16. Microstructure of the alloy isothermally transformed for 5 h at (a) 750 °C, near the centre of the samples containing graphite and ferrite, when the cooling rate is slower. (b) 700 °C and (c) 750 °C, the structure near the surface edges, showing pearlite and allotriomorphic ferrite.

less stable. This is the basis for example of grey cast - iron as opposed to white cast-iron which has a low silicon concentration.

3.7.2. 750 °C and 700 °C

The microstructures contained a mixture of ferrite and a small amount of graphite (Fig. 16a) following transformation at either 750 °C and 700 °C, alongside pearlite close to the edges of the sample (Figs. 16b and c). Thermodynamic calculations predict that cementite can form at temperatures up to 800 °C (Fig. 2a). Nonetheless when graphite is allowed to exist, the calculations suggest 3 vol.% [19,20] graphite and cementite is excluded as a stable phase.

3.7.3. 650 °C

Transformation at 650 °C resulting in a mixture of pearlite with a small amount of allotriomorphic ferrite (Fig. 17). If graphite is excluded from the calculations, the only phases predicted from thermodynamic modelling are 87 vol.% ferrite, 13 vol.% cementite and 0.15 vol.% molybdenum carbide, Mo_2C. However, Mo_2C was not identified by X - ray diffraction, perhaps because the precipitate fraction is small. However, cementite particles do not form a lamellar structure except in a very small region highlighted in Fig. 17c, the reason is that large cementite plates breaks down after prolonged heating; small spherical segments of cementite, or spheroidite are formed.

To test this, sample that were held at 650 °C for only 5 min or 90 s before cooling to ambient temperature, showed the classical pearlite lamellar Fig. 17f, with progressive spheroidisation as the time spent at 650 °C increased Fig. 17d.

Fig. 18 shows an expansion at the beginning of the hold due to the ferrite transformation Fig. 19, followed by a contraction due to pearlite formation. However, there is a significant increase in the strain at longer times. The reasons for this are not clear but one possibility is that the pearlite does not initially form with its equilibrium composition because of the speed of transformation. Subsequent changes towards equilibrium may occur during prolonged holding at the transformation temperature. In particular, the trade - off between the rejection of (Ni, Al, Si) and enrichment of Mo. As Mo has a bigger atomic size as compared to Ni, Al and Si we can observe an initial drop and subsequent increase in strain

value while isothermally holding for longer time. This hypothesis has been partially confirmed using EDX points scanning and the comparison of equilibrium and para-equilibrium[2] calculations Fig. 20.

3.7.4. 600 °C and 550 °C

A significant change happens when the transformation temperature is decreased below 600 °C (Fig. 21). Both transformed samples show structure consisting of a martensite and spherodised cementite particles in ferrite. The ferrite has fully recrystallised into equiaxed grains. Thermodynamic calculations suggest that a small amount of austenite ought to remain untransformed at both 600 °C and 550 °C, yet this was not detected using XRD. Cementite and ε carbide peaks are highlighted in the sample transformed at 550 °C (Fig. 22). Furthermore, the phase fractions of cementite and ferrite following Rietveld analysis of XRD data are in excellent agreement with thermodynamic calculations in Fig. 2a with ≈ 85 vol.% ferrite and ≈ 15.0 vol.% cementite, in the two cases.

3.7.5. 500 °C – 400 °C

Plate-shaped ferrite consistent with displacive transformation (Fig. 23) occurs when the alloy is transformed between 500 °C and 400 °C. Cementite precipitation is restrained because of the existence of silicon and aluminium that are unable to partition at relatively low transformation temperature [e.g., Refs. [30–33]]. The partitioning of carbon into austenite allows it to be retained to ambient temperature (Fig. 24).

3.7.6. Below 400 °C

Isothermal transformation at less than 400 °C, prompts fine plates of bainitic ferrite separated by films or blocks of retained austenite (Figs. 25–27). No other phases were present as confirmed by XRD (Fig. 24). The amount of retained austenite for all of the isothermal

---

[2] Substitutional alloying elements are unable to partition during the time scale of the experiment compares with equilibrium where substitutional alloying elements diffuses at higher temperature.
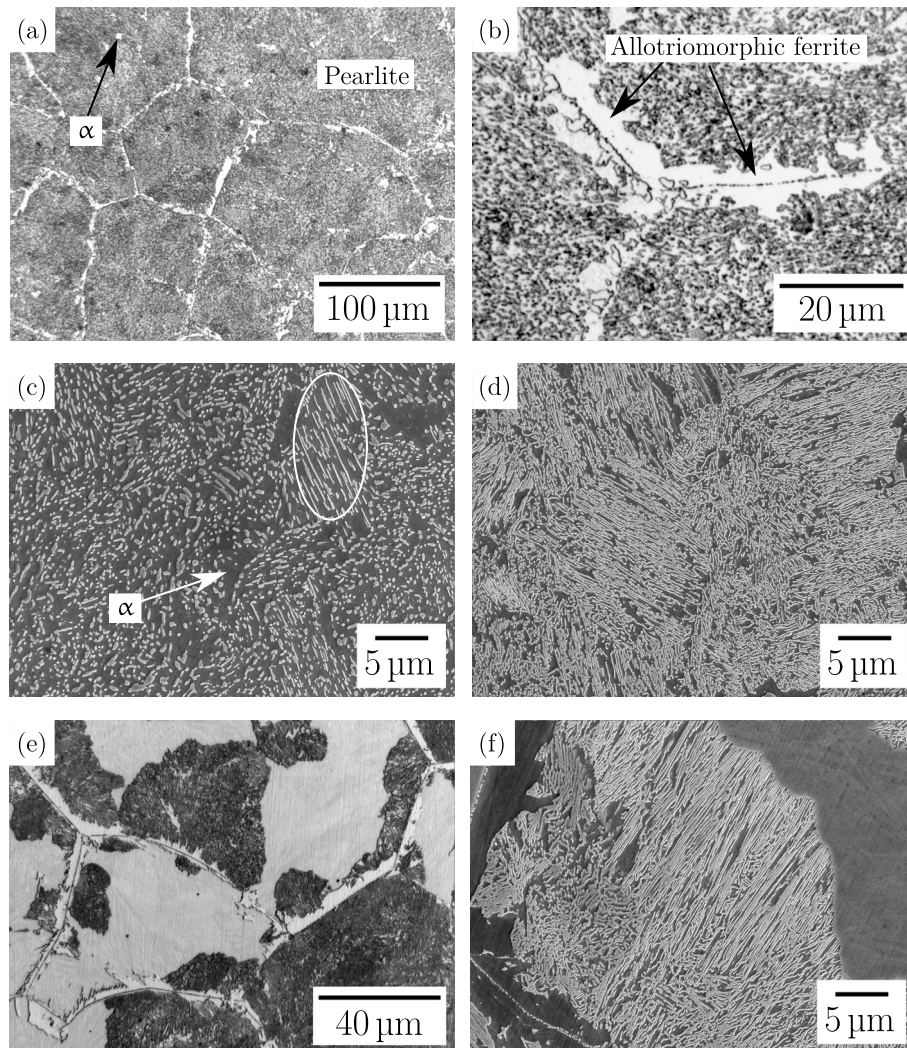
Fig. 17. Microstructure obtained after isothermal transformation at 650 °C for 5 h, (a) and (b) showing mostly pearlite with allotriomorphic ferrite at prior austenite grain boundaries. (c) Classical pearlite highlighted, the cementite particles in the other regions do not form a lamellar structure. (d) Held for 5 min, shows structure of short lamellae. (e) and (f) held for 90 s, shows cooperative growth of pearlite.
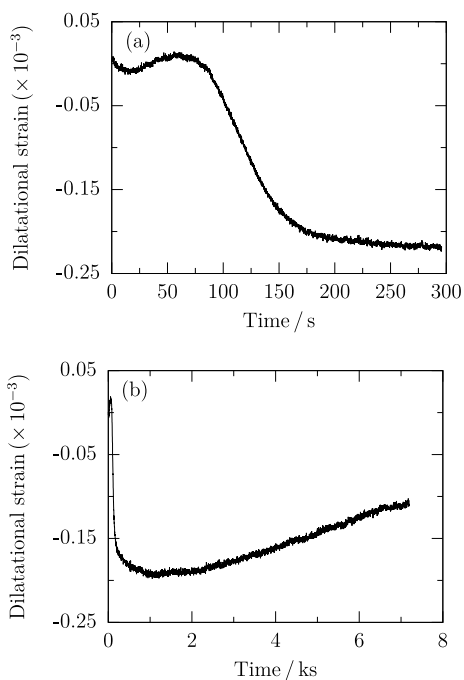
Fig. 18. Dilatational strain measured during isothermal holding at 650 °C for (a) 5 min; (b) 2 h, the strain does not become horizontal due to trade-off of elements.
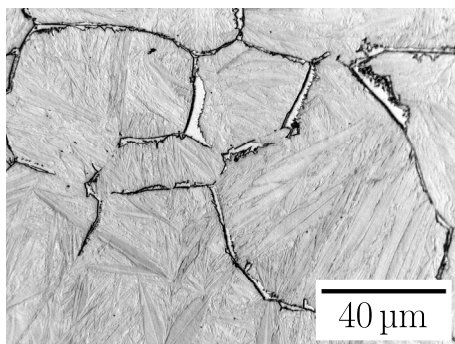

Fig. 19. Microstructure of the alloy after isothermal transformation at 650 °C for 30 s, showing mostly martensite with allotriomorphic ferrite at prior austenite grain boundaries.
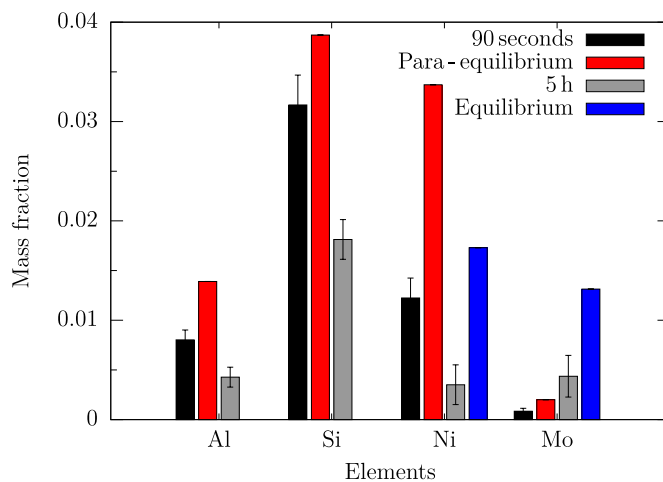

Fig. 20. Calculated and measured mass fraction of components in cementite phase after isothermal transformation at 650 °C at the time indicated.
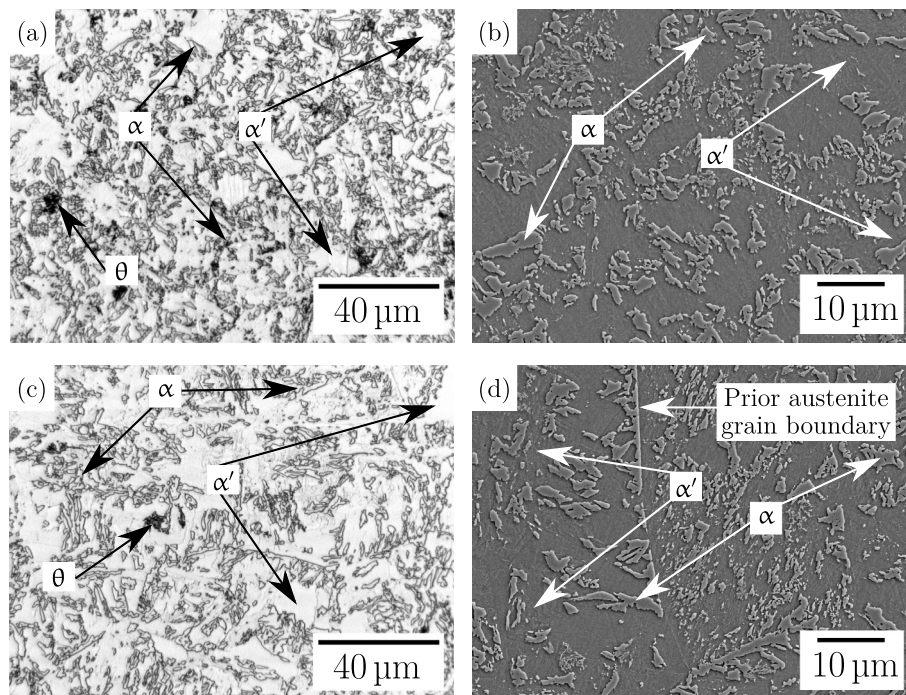
Fig. 21. Microstructure of the alloy transformed at (a) and (b) 600 °C for 6 h; (c) and (d) 550 °C for 6.5 h. Ferrite grains formed on prior austenite grain boundaries scattered with areas of martensite and smaller dark regions of cementite.
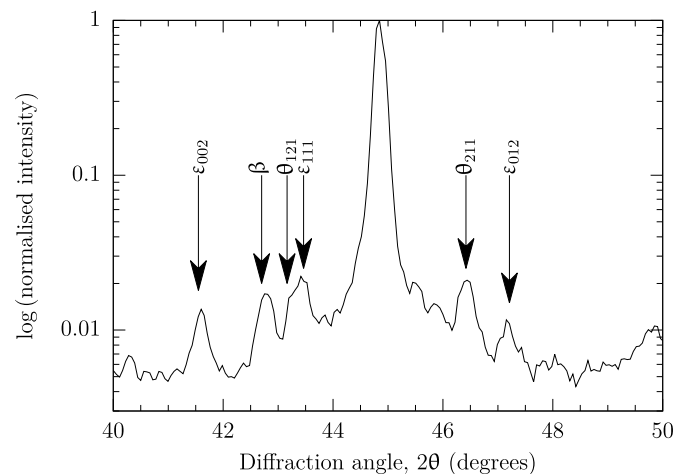

Fig. 22. XRD data for the alloy transformed at 550 °C, shows ϵ carbide and cementite peaks, with peak due to CuK_β radiation.

transformation temperatures is shown in Fig. 28. A microstructure such as this, where fine plates of bainitic ferrite are separated by films of austenite, is in many respects desirable from the perspective of mechanical properties [34–41].

Decreasing the isothermal transformation temperature leads to more refined structure. Using calibrated scanning electron micrographs, the intercepts perpendicular to the long axis of the plates were measured and stereologically corrected [42] to obtain the true widths (Fig. 29).

4. Conclusions

The presence of austenite in nanostructured bainitic steels is mostly responsible for the toughness. However, the austenite is metastable and previous work has demonstrated that it decomposes into cementite and ferrite upon heating. This decomposition makes the material brittle and weak. Likewise the strength of the microstructure relies upon its scale – the plates of bainite get finer as the transformation temperature is decreased and the strength of the austenite increased [25,43]. The alloy investigated here was able to form a finer bainitic structure following transformation at 260 °C and produced the desired microstructure. In the course of the investigations to find the optimum heat treatments, a number of other phenomena were discovered:

- The pearlite obtained during rapid transformation at 650 °C does not form with its equilibrium chemical composition, and yet, all models of pearlite growth, without exception, assume the existence of local equilibrium at the common front with the austenite.
- The alloy has a tendency to form graphite during heat treatment at temperatures in excess of 850 °C. The thermodynamic stability of graphite at elevated temperatures contributes to its formation.
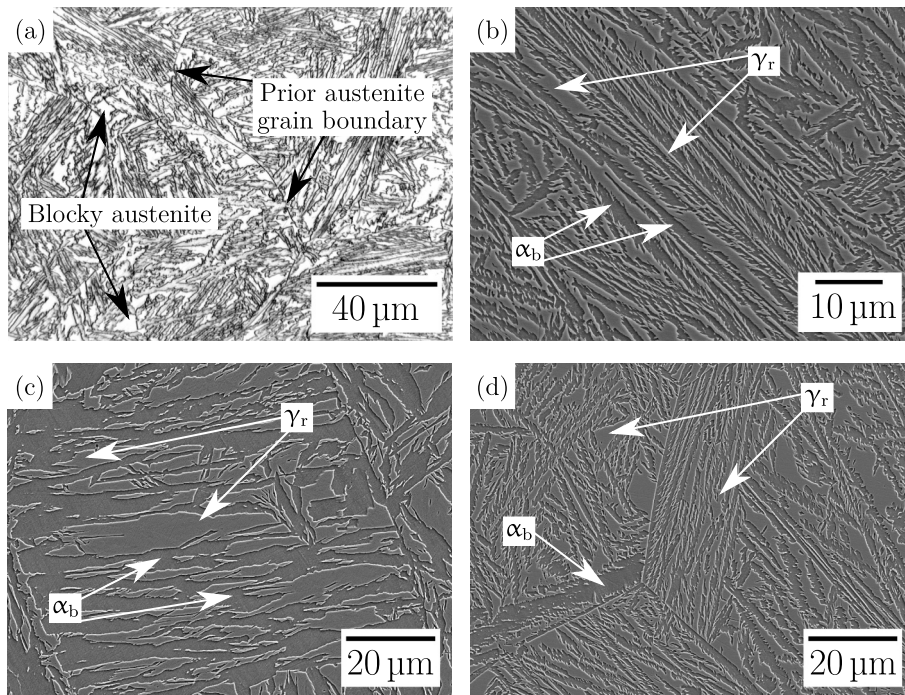
Fig. 23. Alloy transformed at (a) and (b) 500 °C, (c) 450 °C and (d) 400 °C. The microstructure consists of films of bainitic ferrite, and retained austenite with regions of blocky austenite.
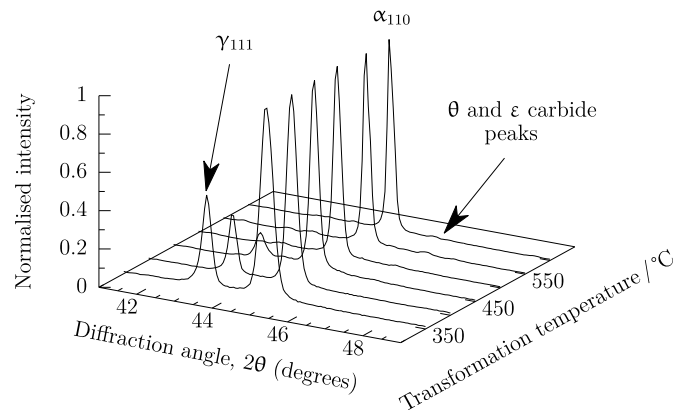

Fig. 24. Isothermal transformation X - ray diffraction peaks at the temperatures indicated. Retained austenite peaks increases in height as transformation temperature decreases, whereas carbide peaks become smaller and then vanish for transformation at or below 400 °C.
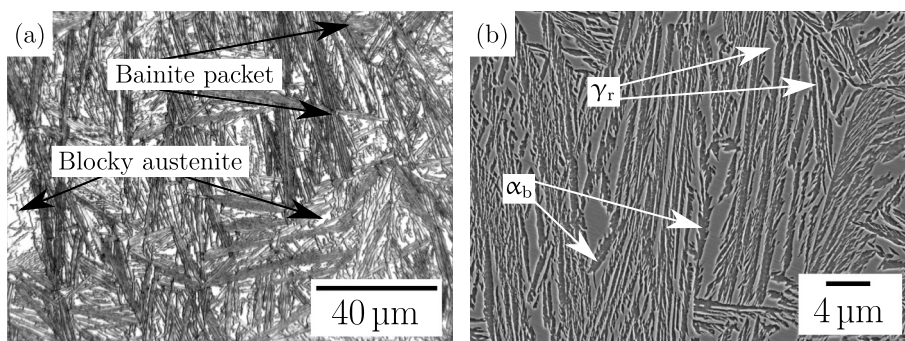

Fig. 25. Microstructure of the alloy isothermally transformed at 350 °C for 12 h, blocks of austenite between parallel sheaves of bainite, which also contain films of austenite.
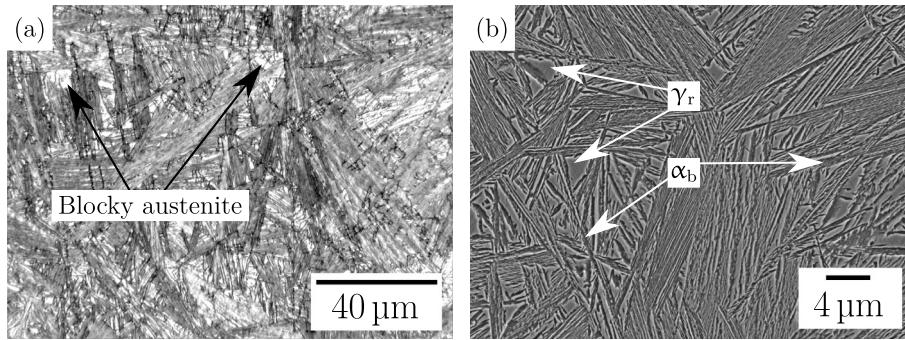
Fig. 26. Microstructure of the alloy isothermally transformed at 300 °C for 12 h. The microstructure is profoundly the same as that formed by transformation at 350 °C (Fig. 25), but with finer microstructure.
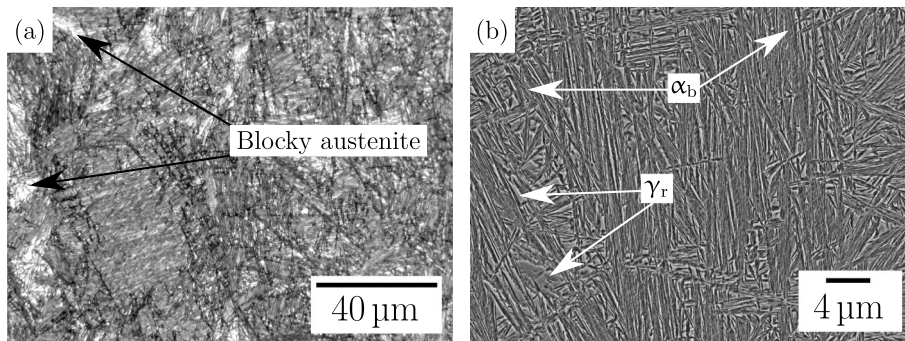

Fig. 27. Microstructure of the alloy isothermally transformed at 260 °C for 12 h. Blocks of austenite become finer, consistent with the isothermal transformation at lower transformation temperature.

Fig. 28. Volume fraction of retained austenite obtained via Rietveld analysis of XRD data. As the transformation temperature decreases below 550 °C, the volume fraction of retained austenite increases. Because of the suppression of cementite by the presence of aluminium and silicon. Carbon in this way stays in solution and stabilises austenite.

Fig. 29. Mean lineal intercept plate width of bainitic ferrite and film austenite after isothermal transformation at the temperatures indicated, stereologically - corrected "$\frac{1}{2}\pi P_W$", where P_W is the plate width [42]. (a) Larger plate widths at higher transformation temperaturer and (b) almost identical finer scale at 325 °C and below. The error bars represent one standard deviation over at least ten values.

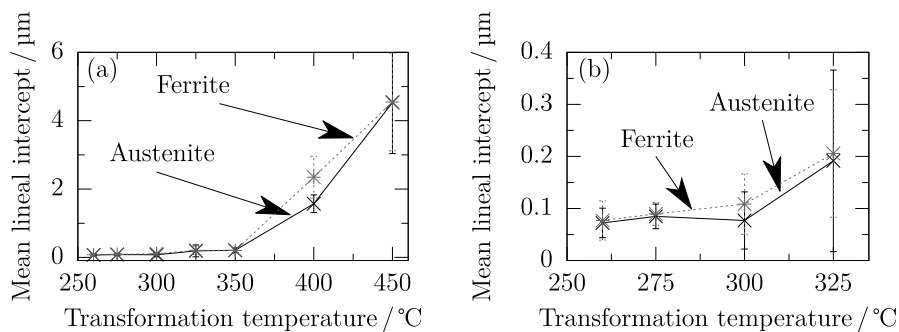Graphite has a lower energy state compared to other carbon-rich phases, such as cementite, which makes it more favourable under certain conditions. At temperatures above 850 °C, the alloy's composition and the kinetics of the transformation play crucial roles in determining the formation of graphite.

It's important to note that the tendency to form graphite during heat treatment is not necessarily detrimental in all cases. In fact, the controlled formation of graphite can be desirable for specific applications. For example, in cast iron, graphite flakes impart enhanced machinability, damping properties, and thermal conductivity. However, in other alloys, such as steels, the formation of graphite can be undesirable, leading to reduced mechanical strength, decreased toughness, or compromised dimensional stability. Therefore, understanding the alloy's intended use and its response to heat treatment is crucial in determining whether the tendency to form the graphite is advantageous or requires modification.

Credit author statement

The author confirms sole responsibility for the following: study conception and design, data collection, analysis and interpretation of results, and manuscript preparation.

Declaration of competing interest

The authors declare that they have no known competing financial interests or personal relationships that could have appeared to influence the work reported in this paper.

Data availability

Data will be made available on request.

References

[1] H.K.D.H. Bhadeshia, Atomic mechanism of the bainite transformation, J. Heat Treat. Mater. 72 (6) (2017) 340–345.
[2] J. Deliry, Noveau carbure de fer transformation bainitique dans les aciers au carbone silicium, Memoires Scientifiques Rev. Metallurg. 62 (1965) 527–550.
[3] J. Pomey, Revenu de la martensite et reaction bainitique inferieure: cas des aciers au carbone-silicium et des aciers au carbone, Memoires Scientifiques Rev. Metallurg. 63 (1966) 507–532.
[4] E. Kozeschnik, H.K.D.H. Bhadeshia, Influence of silicon on cementite precipitation in steels, Mater. Sci. Technol. 24 (2008) 343–347.
[5] H.K.D.H. Bhadeshia, D.V. Edmonds, Bainite in silicon steels: a new composition-property approach II, Met. Sci. 17 (1983) 420–425.
[6] H.K.D.H. Bhadeshia, D.V. Edmonds, Bainite in silicon steels: a new composition-property approach I, Met. Sci. 17 (1983) 411–419.
[7] F.B. Pickering, Mechanism of bainite formation in low-alloy steels containing up to 0.4% carbon, in: 4th International Conference on Electron Microscopy, Springer Verlag, Berlin, 1958, pp. 626–637.
[8] L.C. Chang, H.K.D.H. Bhadeshia, Austenite films in bainitic microstructures, Mater. Sci. Technol. (1995) 874–881.
[9] F.G. Caballero, H.K.D.H. Bhadeshia, Very strong bainite, Curr. Opin. Solid State Mater. Sci. 8 (2004) 251–257.
[10] H.K.D.H. Bhadeshia, The first bulk nanostructured metal, Sci. Technol. Adv. Mater. 14 (2013), 14202.
[11] G.M.A.M. El-Fallah, H.K.D.H. Bhadeshia, Tensile behaviour of thermally-stable nanocrystalline bainitic-steels, Mater. Sci. Eng., A 746 (2019) 145–153.
[12] G.M.A.M. El-Fallah, S.W. Ooi, H.K.D.H. Bhadeshia, Effect of nickel aluminide on the bainite transformation in a fe-0.45c–13ni–3al–4co steel, and associated properties, Mater. Sci. Eng., A 767 (2019), 138362.
[13] G.M.A.M. El-Fallah, Structural Evolution during the Plastic Deformation of Nanostructured Steel, PhD thesis, University of Cambridge, 2019.
[14] H.I. Aaronson, H.A. Domian, Partitioning of alloying elements between austenite and proeutectoid ferrite and bainite, TMS-AIME 236 (1966) 781–796.
[15] R.H. Greaves, J.A. Jones, Temper brittleness of steel; susceptibility to temper brittleness in relation to chemical composition, J. Iron Steel Inst. 111 (1925) 241–255.
[16] H.M. Rietveld, A profile refinement method for nuclear and magnetic structures, J. Appl. Crystallogr. 2 (1969) 65–71.
[17] B.H. Toby, R factors in Rietveld analysis: how good is good enough? Powder Diffr. 21 (1) (2006) 67–70.
[18] D.J. Dyson, B. Holmes, Effect of alloying additions on the lattice parameter austenite, J. Iron Steel Inst. 208 (1970) 469–474.
[19] R.H. Davies, A.T. Dinsdale, J.A. Gisby, J.A.J. Robinson, S.M. Martin, MTDATA-thermodynamic and phase equilibrium software from the national physical laboratory, Calphad 26 (2002) 229–271.
[20] SGTE Thermodynamic Database for Steels, 2006, version 4.2.
[21] NPL PLUS Thermodynamic Database, 1993, version 3.02.
[22] T. Okumura, T. Sourmail, MTTTData. Available from, http://www.msm.cam.ac.uk/map/steel/programs/MTTTDATA.html, 2004.
[23] P. Rubin, R. Larker, E. Navara, M.L. Antti, Graphite formation and dissolution in ductile irons and steels having high silicon contents: solid-state transformations, Metallogr. Microst. Anal. 7 (5) (2018) 587–595.
[24] Hong Seok Yang, H.K.D.H. Bhadeshia, Uncertainties in dilatometric determination of martensite start temperature, Mater. Sci. Technol. 23 (2007) 556–560.
[25] S.B. Singh, H.K.D.H. Bhadeshia, Esitmation of bainite plate-thickness in low-alloy steels, Mater. Sci. Eng. 245 (1998) 72–79.
[26] H.K.D.H. Bhadeshia, Hard bainite, Miner. Metals Mater. Soc. 1 (2005) 469–484.
[27] Francisca G. Caballero, H.K.D.H. Bhadeshia, Very strong bainite, Curr. Opin. Solid State Mater. Sci. 8 (2004) 251–257.
[28] Carlos García-Mateo, Francisca G. Caballero, H.K.D.H. Bhadeshia, Low temperature bainite, J. Phys. IV 112 (2003) 285–288.
[29] DoITPoMS - Micrograph Library, Avaible from, University of Cambridge, 2015, http://www.doitpoms.ac.uk/miclib/index.php.
[30] P.J. Jacques, E. Girault, T. Catlin, N. Geerlofs, T. Kop, Sybrand van der Zwaag, F. Delannay, Bainite transformation of low carbon Mn–Si TRIP-assisted multiphase steels: influence of silicon content on cementite precipitation and austenite retention, Mater. Sci. Eng. 273–275 (1999) 475–479.
[31] Jae Hoon Jang, In Gee Kim, H.K.D.H. Bhadeshia, Substitutional solution of silicon in cementite: a first-principles study, Comput. Mater. Sci. 44 (2009) 1319–1326.
[32] E. Kozeschnik, H.K.D.H. Bhadeshia, Influence of silicon on cementite precipitation in steels, Mater. Sci. Technol. 24 (2008) 343–347.
[33] J. Gordine, I. Codd, The influence of silicon up to 1.5 wt% on the tempering characteristics of a spring steel, J. Iron Steel Inst. 207.1 (1969) 461–468.
[34] Sangeeta Khare, K.Y. Lee, H.K.D.H. Bhadeshia, Carbide-free bainite: compromise between rate of transformation and properties, Metall. Mater. Trans. 41 (2010) 922–928.
[35] Carlos García-Mateo, G. Francisca, Caballero. Understanding the mechanical properties of nanostructured bainite, in: NANOBAIN: Significant Extension of the Bainite Transformation Theory, 2015, pp. 35–65.
[36] H.K.D.H. Bhadeshia, Nanostructured bainite, in: Proceedings of the Royal Society A: Mathematical, Physical and Engineering Sciences, vol. 466, 2009, pp. 3–18.
[37] Hala S. Hasan, Mathew James Peet, Marie-Noelle Avettand-Fénoël, H.K.D.H. Bhadeshia, Effect of tempering upon the tensile properties of a nanostructured bainitic steel, Mater. Sci. Technol. 615 (2014) 1–22.
[38] H.K.D.H. Bhadeshia, Properties of fine-grained steels generated by displacive transformation, Mater. Sci. Eng. 481–482 (2008) 36–39.
[39] Behzad Avishan, Carlos García-Mateo, L. Morales-Rivas, S. Yazdani, Francisca G. Caballero, Strengthening and mechanical stability mechanisms in nanostructured bainite, J. Mater. Sci. 48 (2013) 6121–6132.
[40] I. Lonardelli, M. Bortolotti, W. van Beek, L. Girardini, M. Zadra, H.K.D.H. Bhadeshia, Powder metallurgical nanostructured medium carbon bainitic steel : kinetics , structure , and in situ thermal stability studies, Mater. Sci. Eng. 555 (2012) 139–147.
[41] Mathew James Peet, Transformation and Tempering of Low-Temperature Bainite, PhD thesis, University of Cambridge, 2010.
[42] C. Mack, M.S. Bartlett, On clumps formed when convex laminae or bodies are placed at random in two or three dimensions, Math. Proc. Camb. Phil. Soc. 52 (1956) 246.
[43] H.K.D.H. Bhadeshia, Developments in martensitic and bainitic steels: role of the shape deformation, Mater. Sci. Eng. 378A (2004) 34–39.